RSC Advances

ROYAL SOCIETY OF CHEMISTRY

www.rsc.org/advances

Journal Name

RSCPublishing

ARTICLE

High Performance Solid Polymer Electrolyte with Graphene Oxide Nanosheets

Cite this: DOI: 10.1039/xoxxoooooox

Mengying Yuan[a], Jeremy Erdman[a,c], Changyu Tang[b], Haleh Ardebili[a]*

Received ooth January 2012,
Accepted ooth January 2012

DOI: 10.1039/xoxxoooooox

www.rsc.org/

Two dimensional graphene oxide (GO) sheets with high surface area and excellent mechanical properties are introduced into solid polyethylene oxide/lithium salt electrolyte. Nearly two orders of magnitude improvement in ion conductivity and 260% increase in tensile strength of the polymer electrolyte are achieved with only 1 wt% GO content. GO fillers show improved thermo-mechanical stability of the polymer electrolyte and they appear to significantly enhance the performance of the Li ion battery.

Introduction

Conventional lithium-ion batteries containing organic liquid electrolytes are associated with inherent disadvantages of leakage, solid electrolyte interphase (SEI), dendrite growth, electrical shorting, thermal runaway, and in severe cases, catastrophic fire hazards.[1-3] Solid polymer electrolytes (SPEs) have emerged as safer alternatives that offer significant benefits including higher thermal and electrochemical stability, suppression of dendrite growth, and thin film manufacturability[4] leading to tantalizing applications like flexible and stretchable batteries. However, the low ion conductivity of solid polymer electrolytes, especially at room temperature remains a challenge. The incorporation of ceramic nanofillers (i.e. Al_2O_3, SiO_2, γ-$LiAlO_2$, and TiO_2) into polymer electrolyte has shown to improve ion conductivity without compromising the mechanical properties, thus making polymer nanocomposite electrolytes (PNEs) very attractive for energy storage applications.[5-15] The enhanced properties are generally attributed to the large surface-to-volume ratio, robust mechanical strength, specific surface chemistry, and interfacial effects of the nanofillers. For example, compared to their micro-sized counterparts, nano-sized alumina and silica with large surface densities are more efficient in improving the ionic conductivity of polyethylene oxide (PEO) electrolyte by suppressing the crystallization of PEO.[16-18] Our previous work demonstrated that the nano-sized clay-CNT improved both the ionic conductivity and the mechanical strength of the polymer electrolyte. [19]

Two dimensional, single-atomic-thickness graphene oxide (GO) sheets with their ultra-large surface area, and excellent mechanical and electrical insulating properties, can be promising filler candidates for improving the ionic conductivity and mechanical properties of polymer electrolytes.[20-23] Few studies have investigated the incorporation of GO sheets in PEO host. [24-26].

In this study, we have fabricated solid PEO-$LiClO_4$-GO polymer nanocomposite electrolyte (Scheme 1) by solution blending and evaporation casting and investigated the properties of the electrolyte. The resultant composite electrolyte with 1 wt% GO shows about two orders of magnitude enhancement in ion conductivity (~10^{-5} S·cm^{-1}) compared to that of pure polymer electrolyte fabricated in our lab (~10^{-7} S.cm^{-1}). The enhancement of ion conductivity with the addition of GO fillers can be mainly attributed to the reduced crystallinity and increase in polymer chain mobility as indicated by the lower Tg measurements of the GO filled polymer electrolyte, potential formation of GO ion transport channels, and increase in salt dissociation. Furthermore, the tensile strength of the polymer composite electrolyte was found to increase by 260% compared to that of pure polymer electrolyte which can be attributed to the superior mechanical properties of the GO sheets and the strong interaction between the GO and the surrounding PEO host. Moreover, GO fillers appear to improve the thermo-mechanical stability of polymer electrolyte and overall, the Li ion battery with GO filled polymer electrolyte shows enhanced performance.

Results and discussion

Scanning electron microscopy (SEM) was used to observe the morphology of GO nanosheets (Figure 1a) and the PEO/GO composite electrolyte (Figure 1b). Figure 1a reveals the shape and size of the GO layers. The cross-sectional image of PEO electrolyte with 0.5 wt% GO content (Figure 1b) shows a wave-like morphology and the GO sheets appear to be well integrated within the polymer matrix. With further increase in GO content (5 wt%) the GO nanosheets form aggregates in the matrix due to their large surface energy and close proximity.

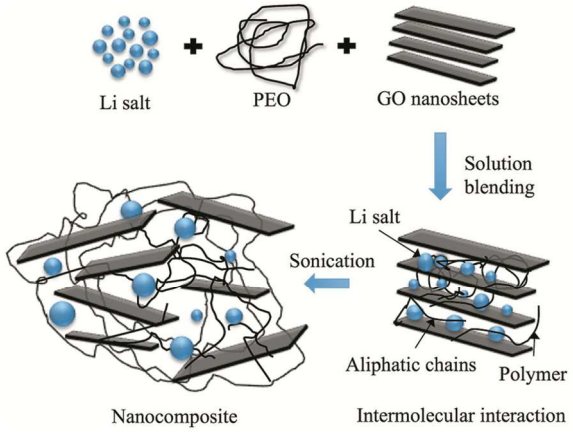

Scheme 1 The schematic of PEO/GO/Li salt membrane

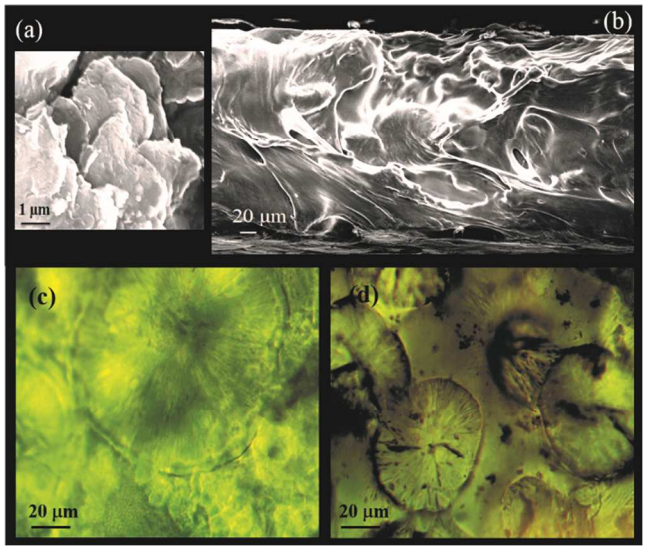

Figure 1 Scanning electron microscopy (SEM) of (a) graphene oxide (GO) (b) cross-section of 0.5 wt. % GO /PEO-Li polymer electrolyte and the polarized light microscopy (PLM) images of (c) filler-free polymer electrolyte and (d) 5 wt. % GO/PEO-Li polymer electrolyte

The 2-D GO sheet has a number of oxygenated functionalities including epoxy, hydroxyl, and carboxyl groups, which can exhibit good affinity for Li^+ transport. As the GO content increases (1wt%) the GO sheets can interconnect to form a network that can facilitate continuous ion conducting channels within the polymer composite electrolyte.[27-30] Our experimental data shows about two orders of magnitude enhancement of ionic conductivity at ambient temperature with only 1 wt% GO fillers. In addition to the potential formation of GO ion conducting network, the large enhancement in ionic conductivity of the PEO/GO electrolyte can be attributed to (i) higher Li ion mobility associated with higher polymer segmental mobility due to free-volume expansion and reduced crystallinity of the polymer matrix and (ii) increase in mobile carrier concentration due to filler-induced dissociation of the Li salt.[31]

Polarized light microscopy (PLM) was used to examine the crystallinity of the PEO/GO electrolyte films. Spherical crystals (spherulites) can be seen in the PLM images of pure PEO electrolyte as shown in Figure 1c indicating the semi-crystalline nature of PEO. Figure 1d shows the PLM image of PEO/GO with 5% GO content. The addition of GO filler appears to decrease the size and number of the spherical crystals. The gradual reduction in the size of the PEO crystals can be further observed from the PLM images of the PEO composites (0.5%, 1%, 5%) provided in Figure S1.

Figure 2a shows the ionic conductivity of PEO electrolytes obtained from Nyquist plots (Figure S2) with various GO contents at room temperature. The ionic conductivity of the PEO composite electrolyte is observed to increase with GO content, and reaches a maximum conductivity at 1 wt% GO content of about 2×10^{-5} S·cm^{-1} showing close to two orders of magnitude conductivity enhancement relative to that of pure PEO electrolyte. As the GO content increases beyond 1%, the ionic conductivity of the composite electrolyte appears to decline. Figure 2b depicts the temperature dependency of ionic conductivity of PEO with 1wt% GO. To investigate the effectiveness of GO in the presence of small amount of plasticizer, the ion conductivities of pure and 1%GO filled PEO, both with 5% plasticizer ($LiPF_6$ in ethylene carbonate (EC) + dimethyl carbonate (DMC) + diethyl carbonate (DEC)), were evaluated (Figure S5). The ion conductivity of the plasticized PEO/GO (1×10^{-4} S·cm^{-1}) shows two orders of magnitude improvement compared to that of unfilled plasticized PEO (4×10^{-6} S·cm^{-1}).

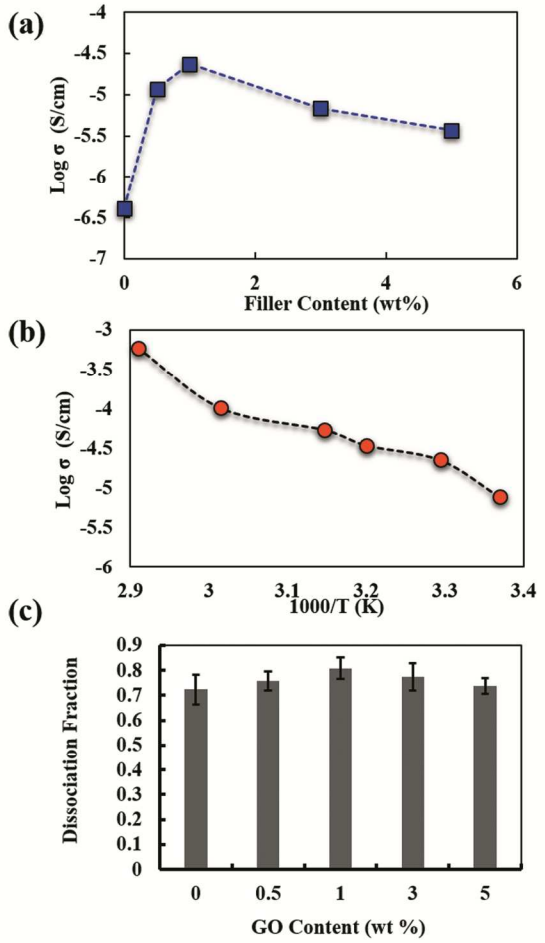

Figure 2(a) Ionic conductivity (σ) at room temperature (b) temperature dependence of ion conductivity (1 wt% GO

content) and (c) Li salt dissociation fractions of polymer electrolyte films.

The ionic conductivity of an electrolyte is related to the number of the charge carriers (n_i), ionic charge (z_i), and ion mobility (μ_i) in the electrolyte expressed as follows: [32]

$$\sigma = \sum n_i z_i \mu_i \quad (1)$$

In the polymer electrolyte, n_i corresponds to the concentration of free ions involved in the ionic transport and μ_i (ion mobility) is strongly influenced by the polymer chain segmental mobility. Thus, it is necessary to analyse the mechanisms of the ionic conductivity enhancement in the GO-filled PEO electrolyte with respect to the latter two factors, namely, the concentration of the free ions and the ion mobility.

Figure 2c shows the fraction of free ClO_4^{-1} calculated from the Fourier Transform Infrared (FTIR) spectra for pure PEO and its nanocomposites of various GO contents. The method of calculation of dissociation fraction is discussed in the Experimental Section and the FTIR spectra are shown in Figure S4. It can be seen from Figure 2c that the dissociated lithium salt ions in pure PEO count for about 70%. With the incorporation of GO sheets in the polymer electrolyte, the free ions increase to a maximum of 80% at 1 wt% GO content. This suggests that the GO sheets can effectively facilitate the dissociation of lithium salt by weakening the bond between the contact ion pairs, resulting in the increased charge carrier concentration. There are no obvious changes in the degree of lithium salt dissociation upon further increase in GO content beyond 1 wt%.

The mobility of the polymer chains was investigated by thermal analysis of solid PEO-$LiClO_4$-GO using differential scanning calorimetry (DSC). The DSC curves are shown in Figure S3. The melting point (Tm) and the glass transition temperature (Tg) of the polymer electrolyte films are shown in Figure 3a. The crystalline fraction (χc) shown in Figure 3b is calculated by the following equation: [33]

$$\chi_c(\%) = \left(\Delta H_m / \Delta H_m^0\right) \times 100 \quad (2)$$

where, ΔH_m is the fusion heat of PEO/Li-xGO (x=0, 0.5%, 1%, 3%, 5%), and ΔH_m^0 is the melting heat of pure PEO crystalline, 213.7 J/g (100% crystalline). [34] The fusion heat (ΔH_m) can be calculated from the integral area of the DSC curves.

Based on the DSC results, the melting temperature and crystallinity of the nanocomposite electroyte decrease with the addition of GO nanosheets. This suggests that the crystallization of the PEO chains can be effectively disrupted by the presence of GO nanosheets with ultra-large surface area. In addition, the oxygenated functionalities on GO sheets also can play a key role in the formation of strong interaction between GO and PEO. [35] The tertiary alcohols and epoxy (1,2-ethers) on the GO basal planes can interact with the PEO ether groups by forming hydrogen bonding.

Upon the addition of lithium salt, the Tg of pure PEO film increased from -60 to -20℃. This phenomenon is referred to as the "salt effect" and is attributed to the formation of complexes between PEO and ClO_4^{-1}.[7] Upon the addition of GO nanosheets, the Tg of the polymer electrolyte decreases. A minimum Tg of about -35℃ is reached at 5 wt. % of GO content, which is much lower than the Tg at 1 wt% filled electrolyte. The compact molecular packing and crystallization of the solid PEO are greatly disturbed by the presence of GO sheets leading to the lower Tg values. In general, a low Tg indicates increase in free volume and larger amorphous regions in the polymer matrix and subsequent higher polymer chain mobility. Due to intimate relations between ion conductivity, polymer segmental mobility, free volume and Tg, a maximum ionic conductivity is expected to be realized at the lowest Tg which is at 5 wt% GO content in our polymer nanocomposite system. However, the maximum ionic conductivity of PEO electrolyte was observed at 1 wt% GO and beyond this content, the ion conductivity declines. This suggests adverse filler effects at higher GO contents that can counteract the influence of reduced Tg and the associated increase in polymer chain mobility. These adverse effects can consist of filler aggregation, diffusion tortuosity, and ion trapping. [36]

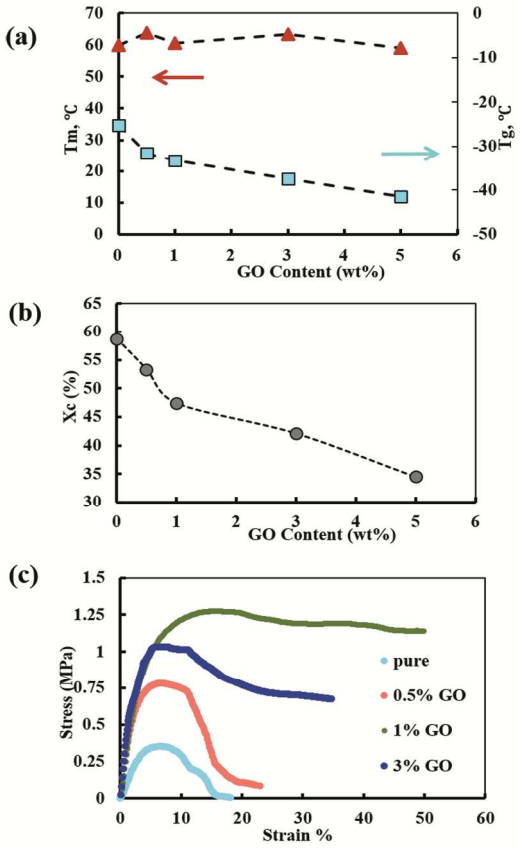

Figure 3(a) Melting point (Tm) and glass transition temperature (Tg) (b) crystalline fraction (χc) and (c) stress-strain curves of polymer electrolyte films.

The stress/strain curves for the polymer electrolytes are presented in Figure 3c. The 1 wt% GO electrolyte film shows an ultimate tensile strength of 1.27 MPa indicating more than 260% improvement in the tensile strength of the pure polymer electrolyte (0.35 MPa). Stress–strain measurements show a large enhancement of the Young's modulus and of the yield-point stress when passing from filler-free to nanocomposite polymer electrolytes. Here, the active nanocomposite particles serve as both filler and "tie molecules," thus improving the adhesion between the polymer chains. The PEO/GO composite

membranes at lower GO contents (0.5 and 1 wt. %) exhibit excellent tensile strength and % elongation properties.

Figure 4 shows the thermo-gravimetric analysis (TGA) of pure and GO filled polymer electrolyte where no apparent difference can be observed. Figure 5 shows the thermal expansion of pure and 1%GO filled PEO. GO fillers seem to improve the thermo-mechanical stability of polymer electrolyte attributed to GO's strong "tie molecules".

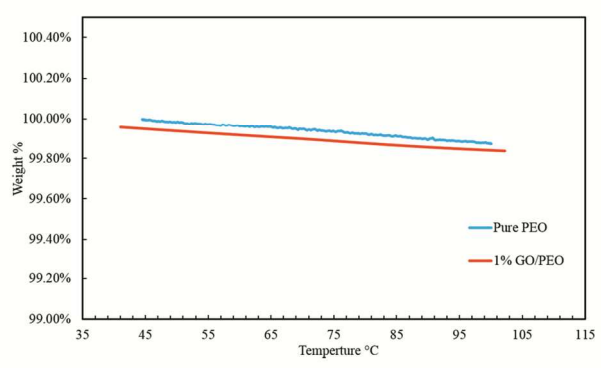

Figure 4 The thermogravimetric analysis (TGA) of pure PEO and GO filled PEO polymer electrolyte films.

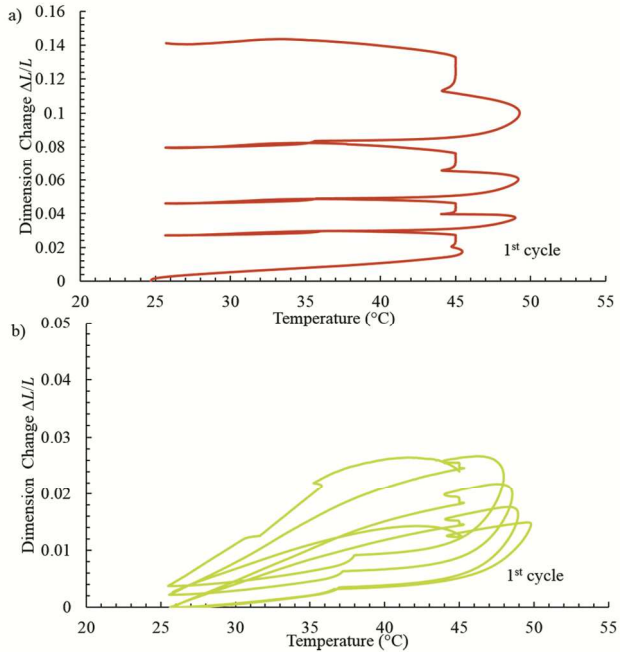

Figure 5 The thermo-mechanical analysis (TMA) of (a) pure PEO and (b) PEO/GO polymer electrolyte films.

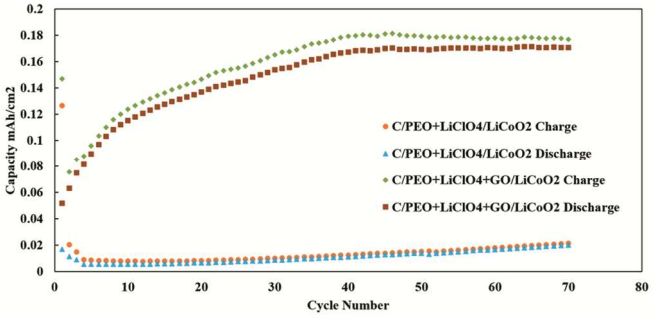

Figure 6 Capacity versus cycle number of C/PEO+$LiClO_4$/$LiCoO_2$ and C/PEO+$LiClO_4$+GO/$LiCoO_2$ cells cycling.

The Li ion coin cell battery performance with GO filled polymer electrolyte is presented in Figure 6. The battery with pure solid polymer electrolyte shows poor capacity attributed mainly to the poor ionic conductivity of the electrolyte. The GO fillers in the electrolyte appear to noticeably improve the performance of the battery where the area capacity reaches 0.17 mAh/cm^2. The reasonable value of the surface area capacity of the battery demonstrates the effectiveness of the PEO/GO polymer electrolyte for thin film batteries. The mass density of the cathode material is 0.012g/cm^2. Since the battery contains a commercial electrode that is more compatible with liquid than solid electrolyte, the mass capacity of the battery is relatively low. This capacity can be significantly improved by using a more suitable (thinner and lower density) electrode. The design and optimization of electrode material that is compatible with solid polymer electrolyte is beyond the scope of this study, and can be pursued in future studies for the effective utilization of the GO filled polymer electrolyte in thin film battery applications.

The impedance spectroscopy of the battery with pure and GO filled polymer electrolyte is shown in Figure 7. The impedance spectroscopy is fitted with equivalent circuits as shown in the inset of Figure 7 revealing that the GO fillers can lead to internal impedance improvements including enhancement in charge transfer and interfacial conductivity.

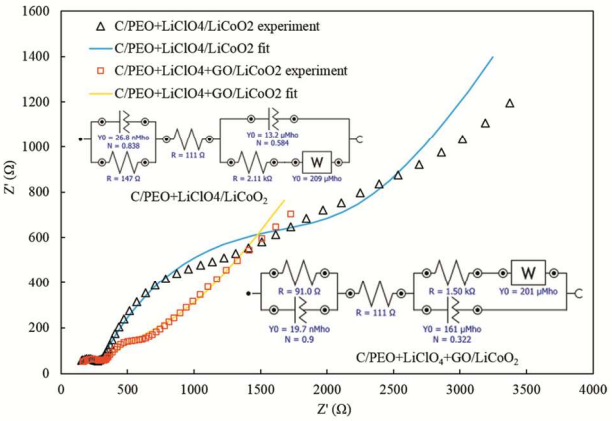

Figure 7 A.C. impedance spectra of C/PEO+$LiClO4/LiCoO_2$ and C/PEO+$LiClO_4$+GO/$LiCoO_2$ cells.

The redox activity of the GO filler was investigated using cyclic voltammetry (CV). The CV curves of both the pure PEO and PEO/1%GO electrolyte based coin cells with Li cobalt oxide as the working electrode versus the lithium metal as the reference electrode were obtained with a scan rate of 0.05 and 0.1 $mV.s^{-1}$, respectively (Figure S6). The redox peaks appear to be the same for both pure and filled PEO indicating the redox inactivity of GO in the PEO electrolyte. Furthermore, the electronic conductivity of the PEO/1%GO was evaluated using DC polarization method (Figure S7 and Table S1) measured to be about 5.6×10^{-8} S/cm demonstrating suitability as a battery electrolyte.

In summary, a novel solid polymer nanocomposite electrolyte with 2D graphene oxide nanosheets was fabricated using solution blending and evaporation casting. We demonstrated a significant enhancement, nearly two orders of magnitude, in ion conductivity with only 1 wt% GO. Furthermore, the electrolyte exhibits excellent mechanical properties with over 260% increase in tensile strength. Battery performance appears to be noticeably improved with GO filled polymer electrolyte. GO fillers also show to enhance the thermo-mechanical stability of the polymer electrolyte. Electrochemical, mechanical and thermal characterizations provided fundamental science insights into the mechanisms of enhancement of the polymer electrolyte properties. The novel PEO/GO electrolyte can be a promising electrolyte for next generation safer Li ion batteries and enable special applications such as flexible and stretchable batteries.

Experimental

Preparation of PEO/GO Composite Films. The Li salt powder (0.3 g, Sigma-Aldrich) and the PEO powder (2 g, Mw=100, 000, Sigma-Aldrich) were dissolved in 30 mL acetonitrile in separate bottles. Graphene oxide (GO) powder with layer dimensions of about 0.5-5 microns in length and width and 1.1 ± 0.2 nm in thickness was purchased from Graphene Supermarket. Appropriate amounts of GO (0.5, 1, 3, 5, and 8 wt. %) was added to the bottles and stirred for 6 hours. Then, the solution from both bottles with PEO, GO and Li salt were mixed together and stirred for another 3 hours to obtain the PEO/GO/Li salt solution. The mixed solution was sonicated using a Branson 3510 Sonicator for 25 min and the PEO/GO solutions were poured into different Teflon petri dishes and kept in the oven at 50 ℃ for 24 h until the membranes were dry.

Morphological Characterization. The morphologies of the polymer/GO films were observed by scanning electron microscopy (SEM) using LEO 1525 under an acceleration voltage of 15 kV. The samples were coated with gold to increase the electrical conduction. Polarized light microscopy (PLM) was used to investigate the crystallinity of the PEO films carried out with Advanced EPI Trinocular Infinity Polarizing Microscope 50x-1600x.

Ion Conductivity Characterization. The ion conductivities were determined using complex impedance method carried out by Metrohm Autolab. The samples were sandwiched between two stainless steel electrode discs and the complex impedance spectra were obtained with the frequency response analysis (FRA) module of the Autolab in the frequency range of 1 Hz – 1 MHz.

Salt Dissociation Measurement. The Li salt dissociation fraction was obtained using the Fourier Transform Infrared (FTIR) Agilent Technologies Cary 630. The spectra were collected with MicroLab software and analyzed using Resolutions Pro. The dissociation fraction was obtained as the ratio of the areas under the peaks located in two specific ranges, 620-624 cm^{-1} range representing the dissociated "free" ClO_4^{-1} ions and 630-635 cm^{-1} range representing the ion-pair $LiClO_4$.[37, 38]

Mechanical Testing. The tensile stress/strain measurements were carried out using the Dynamic Mechanical Analysis (DMA) Model Q800 from TA Instruments at room temperature. The preload force was 0.001N and the tensile rate was 2N/min. The specimen dimensions were 18.00 mm in length and 13.00 mm in width.

Thermal Characterization. The thermal properties of PEO/GO electrolyte films were obtained using TA Instruments Q2000 Differential scanning calorimetry (DSC) under nitrogen atmosphere. The weight of the sample and that of the T_{zero} aluminum container pans and lids were taken before and after each thermal scan. The samples were heated to 200℃, cooled to -90℃ and then heated to 200℃ again with heating and cooling rates of 10℃/min and 5℃/min. The glass transition temperature was determined as the mid-point of the step transition from the second heating. The melting and crystallization temperatures (when observed) were defined as the maxima of the melting endotherms and crystallization exotherms, respectively.

Thermogravimetric Analysis (TGA). Pure and 1%GO composite PEO samples were tested with the TA Instruments TGA in the temperature region of 35 to 100℃. The temperature scanning rate was 10 ℃/min.

Thermomechanical Analysis (TMA). Pure and 1%Go composite PEO were tested using the TA Instruments TMA to investigate their thermal stability and expansion. A probe force of 0.05N was applied and the temperature was varied between 25 and 45. Five heat and cool cycles were conducted to assess thermal stability. The temperature scan rate was 3℃/min.

Li Ion Battery Assembly and Testing. Coin cell batteries were assembled inside the glove box with graphite (anode), pure and composite solid PEO electrolyte and Li cobalt oxide (cathode). The anode, cathode and current collector materials were purchased from MTI. A drop of plasticizer ($LiPF_6$ in ethylene carbonate (EC) + dimethyl carbonate (DMC) + diethyl carbonate (DEC)) was deposited on the surface of each electrode during assembly to enhance interfacial contact. The battery components were assembled layer by layer and sealed using a coin cell-crimping machine. The batteries were then subjected to multiple charge-discharge cycles and their capacities were measured using Arbin equipment. Impedance spectroscopy of the batteries was conducted using the frequency response analysis (FRA) module of the Autolab with frequency ranging from 1 Hz to 1 MHz.

Electronic Characterization of PEO/GO. The ionic (t_{ion}) /electronic (t_{ele}) transport numbers of the pure PEO and PEO/1%GO electrolytes were measured using DC polarization method [24,39,40]. A constant voltage of 50 mV was applied across the electrolyte sandwiched between two blocking stainless-steel electrodes, and the polarization current as a function of time was monitored for 1 hour at RT. The electronic conductivity of the PEO/GO was calculated using the electronic transport

number and the respective ionic conductivity obtained from impedance spectra.

Redox Characterization of PEO/GO. Cyclic voltammetry (CV) measurements were performed on both the pure and composite PEO films with 1%GO using Metrohom Autolab at RT. Coin cells were assembled with the pure and GO filled PEO films as electrolytes, Li cobalt oxide as the working electrode and lithium metal as the reference electrode. The voltage scanning rates used were 0.1 $mV.s^{-1}$ and 0.05 $mV.s^{-1}$ for PEO/GO and pure PEO electrolyte based cells, respectively.

Notes and references

[a] Mechanical Engineering Department, University of Houston, Houston, Texas, 77004, U.S.A
[b] Trinity University, One Trinity Place, San Antonio, Texas 78212, U.S.A
[c] Chengdu Green Energy and Green Manufacturing Technology R&D Center, 2nd Tengfei Rd. No.355, Southwest Airport Economic Development Zone, Chengdu, 610207, China

Electronic Supplementary Information (ESI) available: Polarized light microscopy (PLM), complex impedance spectra, differential scanning calorimetry (DSC), fourier transform infrared (FTIR) spectra, cyclic voltammetry (CV), polarization current curves, ionic/electronic transport numbers and electronic conductivities table. See DOI: 10.1039/c000000x/

ACKNOWLEDGMENT

We acknowledge financial support from NSF CAREER (CMMI-1254477) and TcSUH and NSF (EEC 1261981).

REFERENCES

1. J. M. Tarascon, M. Armand *Nature*. 2001, **414**, 359.
2. M. Armand, J. M. Tarascon *Nature*. 2008, **451**, 652.
3. W. H. Meyer *Advanced materials (Deerfield Beach, Fla.)*. 1998, **10**, 439.
4. K. Xu *Chemical Reviews*. 2004, **104**, 4303.
5. K. S. Ji, H. S. Moon, J. W. Kim, J. W. Park *Journal of Power Sources*. 2003, **117**, 124.
6. G. Jiang, S. Maeda, Y. Saito, S. Tanase, T. Sakai *Journal of the Electrochemical Society*. 2005, **152**, A767.
7. J. H. Ahn, G. X. Wang, H. K. Liu, S. X. Dou *Journal of Power Sources*. 2003, **119**, 422.
8. P. P. Prosini, S. Passerini, R. Vellone, W. H. Smyrl *Journal of Power Sources*. 1998, **75,** 73.
9. G. B. Appetecchi, S. Scaccia, S. Passerini *Journal of the Electrochemical Society*. 2000, **147**, 4448.
10. M. C. Borghini, M. Mastragostino, S. Passerini, B. Scrosati *Journal of the Electrochemical Society*. 1995, **142**, 2118.
11. H. Y. Sun, H. J. Sohn, O. Yamamoto, Y. Takeda, N. Imanishi *Journal of the Electrochemical Society*. 1999, **146**, 1672.
12. H. T. Liao, C. S. Wu *Journal of Polymer Science Part B-Polymer Physics*. 2004, **42**, 4272.
13. P. D. Yang, D. Y. Zhao, D. I. Margolese, B. F. Chmelka, G. D. Stucky *Nature*. 1998, **396**, 152.
14. S. H. Chung, Y. Wang, L. Persi, F. Croce, S. G. Greenbaum, B. Scrosati, E. Plichta *Journal of Power Sources*. 2001, **97-8**, 644.
15. F. Croce, B. Scrosati *Journal of Power Sources*. 1993, **43**, 9.
16. F. Croce, F. Bonino, S. Panero, B. Scrosati *Philosophical Magazine B-Physics of Condensed Matter Statistical Mechanics Electronic Optical and Magnetic Properties*. 1989, **59**, 161.
17. B. Kumar, L. G. Scanlon *Journal of Power Sources*. 1994, **52**, 261.
18. J. J. Xu, K. Wang, S. Z. Zu, B. H. Han, Z. X. Wei *Acs Nano*. 2010, **4**, 5019.
19. C. Tang, K. Hackenberg, Q. Fu, P. M. Ajayan, H. Ardebili *Nano letters*. 2012, **12**, 1152.
20. N. A. Kotov, I. Dékány, J. H. Fendler *Advanced Materials.* 1996, **8**, 637.
21. T. Cassagneau, J. H. Fendler *Advanced Materials.* 1998, **10**, 877.
22. N. I. Kovtyukhova, P. J. Ollivier, B. R. Martin, T. E. Mallouk, S. A. Chizhik, E. V. Buzaneva, A. D. Gorchinskiy *Chemistry of Materials.* 1999, **11**, 771.
23. J.T. Paci, T. Belytschko, G. C. Schatz *Journal of Physical Chemistry C.* 2007, **111**, 18099.
24. J. Shim, D. Kim, H. J. Kim, J. H. Lee, J. Baik, J. Lee *Journal of Materials Chemistry A* 2014, **2**, 13873
25. S. Gao, J. Zhong, G. Xue, B. Wang *Journal of Membrane Science* 2014, **470**, 316
26. M. Akhtar, S. Kwon, F. J. Stadler, O. B. Yang *Nanoscale*, 2013, **5**, 5403
27. Y. Cao, C. Xu, X. Wu, X. Wang, L. Xing, K. Scott *Journal of Power Sources.* 2011, **196,** 8377.
28. G. Eda, M. Chhowalla *Advanced Materials*. 2010, **22**, 2392.
29. D. Chen, L. Tang, J. Li *Chemical Society reviews*. 2010, **39**, 3157.
30. D.R. Dreyer, S. Park, C.W. Bielawski, R.S. Ruoff, *Chemical Society reviews*. 2010, **39,** 228.
31. Q. Li, E. Wood, H. Ardebili *Applied Physics Letters*. 2013, **102**, 243903.
32. B. Scrosati *Applications of electroactive polymers*, Chapman & Hall, London 1993, p. 77
33. Li, Z. H., Zhang, H. P., Zhang, P., Li, G. C., Wu, Y. P., and Zhou, X. D. *Journal of Membrane Science*. 2008, **322**, 416.
34. X. Li, S. L. Hsu *Journal of Polymer Science: Polymer Physics Edition*. 1984, **22,** 1331.
35. F. Barroso-Bujans, F. Fernandez-Alonso, J. A. Pomposo, E. Enciso, J. L. G. Fierro, J. Colmenero *Carbon*. 2012, **50,** 5232.
36. F. Croce, G. B. Appetecchi, L. Persi, B. Scrosati *Nature* 1998, **394,** 456.
37. D. R. Dreyer, S. Park, C. W. Bielawski, R. S. Ruoff *Chemical Society reviews*. 2010, **39**, 228.
38. Y.T. Chen, Y.C. Chuang, J.H. Su, H.C. Yu, Y.W. Chen-Yang *Journal of Power Sources*. 2011, **196**, 2802.
39. N. Shukla, A.K.T. *Solid State Ionics*. 2010, **181**, 921.
40. S. R. Mohapatra, A.K.T., R.N.P. Choudhary. *Journal of Power Sources.* 2009, **191**,601.

